Available online at www.sciencedirect.com
ScienceDirect
Proceedings of the Combustion Institute 31 (2007) 447–454
Proceedings of the Combustion Institute
www.elsevier.com/locate/proci

Methane/propane oxidation at high pressures: Experimental and detailed chemical kinetic modeling ☆

Eric L. Petersen [a,*], Danielle M. Kalitan [a], Stefanie Simmons [a], Gilles Bourque [b], Henry J. Curran [c], John M. Simmie [c]

[a] *Mechanical, Materials and Aerospace Engineering, University of Central Florida, Orlando, FL 32816-2450, USA*
[b] *Rolls-Royce Canada 9500 Côte-de-Liesse, Lachine, Province of Quebec, Que., Canada H8T 1A2*
[c] *Chemistry Department, National University of Ireland, Galway, Ireland*

Abstract

Shock tube experiments and chemical kinetic modeling were performed to further understand the ignition and oxidation kinetics of various methane–propane fuel blends at gas turbine pressures. Ignition delay times were obtained behind reflected shock waves for fuel mixtures consisting of CH_4/C_3H_8 in ratios ranging from 90/10% to 60/40%. Equivalence ratios varied from lean ($\phi = 0.5$), through stoichiometric to rich ($\phi = 3.0$) at test pressures from 5.3 to 31.4 atm. These pressures and mixtures, in conjunction with test temperatures as low as 1042 K, cover a critical range of conditions relevant to practical turbines where few, if any, CH_4/C_3H_8 prior data existed. A methane/propane oxidation mechanism was prepared to simulate the experimental results. It was found that the reactions involving $CH_3\dot{O}$, $CH_3\dot{O}_2$, and $\dot{C}H_3 + O_2/H\dot{O}_2$ chemistry were very important in reproducing the correct kinetic behavior.

Keywords: Ignition; Methane; Propane; Shock tube; Chemical kinetics; Fuel blends; High pressure

1. Introduction

The primary fuel for industrial gas turbines is natural gas [1]. The main constituent of natural gas is methane (CH_4), but higher hydrocarbons from ethane (C_2H_6) through to hexane (C_6H_{14}) can be present in different proportions depending on the geographic origin and extraction and transport processes [2]. Conventional industrial gas turbines have been successfully operating on a large composition envelope. As the emission regulations are imposing tighter limits, dry low emission (DLE) industrial gas turbines using lean premix technology are being favoured. The range of compositions that lean premix technology can accommodate depends on the design. Inherent limitations come from the autoignition delay, flame temperature, and flame dynamics [3–5]. The ignition delay of the evolving fuel air mixture inside the premixer, from the point of injection to combustion zone, needs to be much longer than

☆ Supplementary data for this article can be accessed online. See Appendix A.

* Corresponding author. Fax: +1 407 823 0208.
E-mail address: petersen@mail.ucf.edu (E.L. Petersen).

1540-7489/$ - see front matter © 2006 Published by Elsevier Inc. on behalf of The Combustion Institute.
doi:10.1016/j.proci.2006.08.034

the residence time in order to prevent hardware damage. Fuel compositions having a shorter autoignition delay than a predefined limit at relevant operating conditions are therefore excluded. If the fuel composition does not change significantly over time, the flame temperature can be tightly controlled in a narrow band to minimize NO_x and CO emissions. Finally, the stability of the combustion zone is strongly dependent on the flame dynamics, which is a direct function of fuel thermochemistry.

Fundamental measurements of the ignition delay time of methane/propane mixtures, particularly at pressures and concentrations of interest to gas turbines, are therefore important for the design of efficient engines. Such measurements are also essential for homogeneous charge compression ignition engines and for the optimization of chemical kinetics models. Previous studies on the ignition of methane/propane mixtures have been performed mostly using the shock-tube technique and include the works of Lifshitz et al. [6], Crossley et al. [7], Eubank et al. [8], Zellner et al. [9], Frenklach and Bornside [10], Spadaccini and Colket [2], and Lamoureux and Paillard [11]. Most of these studies considered only stoichiometric mixtures and levels of propane addition less than or equal to 10% by volume of the main methane fuel.

Some of the latest studies have considered CH_4/C_3H_8 ignition at pressures up to 40 atm, namely Huang and Bushe [12], but for limited ranges of propane addition and stoichiometry. One methane/propane blend with an 80/20 volume ratio was explored by the authors in a recent study [13] at a pressure of 12 atm and a fuel-to-air equivalence ratio (ϕ) of 0.5. The focus of the present study was on the measurement and detailed kinetics modeling of methane/propane/air ignition delay times over a much wider range of percent C_3H_8 (10–40%), stoichiometry ($\phi =$ 0.5–3.0), temperature (1042–1585 K), and pressure (5–31 atm) than previously covered. Provided in this paper are details on the experimental method and the results of the shock-tube tests, followed by an outline of the chemical kinetics model. The detailed model is then compared to the present data and select results from the literature.

2. Experimental

2.1. Setup and procedure

All experiments were conducted in the stainless steel shock-tube facility described in detail by Petersen et al. [14]. Briefly, the driver length is 3.5 m, and the driven-tube length is 10.7 m; the inner diameter of the driven tube is 16.2 cm. The test temperature was determined from measurements of the incident-shock velocity via five piezoelectric pressure transducers and four time-interval counters. The temperature behind the reflected shock wave was calculated from the shock speed extrapolated to the endwall and the normal shock relations in the usual fashion. At a reflected-shock temperature of 1300 K, the estimated error in this temperature is approximately 10 K [14]. The test mixtures included equivalence ratios of 0.5, 1.0, 2.0, and 3.0, and CH_4/C_3H_8 splits of 90/10, 80/20, 70/30, and 60/40% by volume. The gases were mixed in a separate mixing tank using partial pressures to an accuracy of better than 1% of each volume fraction numerical value. Gas purities were ultra high purity (99.9995%) for the N_2 and O_2, and research grade (99.95%) for the CH_4 and C_3H_8. The test mixtures were introduced into the shock-tube driven section immediately prior to each experiment, and the single aluminum diaphragms were ruptured routinely within a few minutes after filling. Pre-fill driven-section pressures were typically less than 10^{-5} Torr with a leak/outgassing rate below 10^{-3} Torr/min.

Chemiluminescence emission from excited $CH^\star$ radicals near 430 nm and pressure from an endwall-mounted, sub-microsecond piezoelectric pressure transducer were used to monitor the onset of ignition after passage of the reflected shock wave. The $CH^\star$ emission emanated from a window located in the endwall, through a narrow-band filter, and onto a Hamamatsu 1P21 photomultiplier tube in a homemade housing. It has been shown by the authors in previous papers that the chemiluminescence diagnostic applied to the endwall location provides the most reliable measurement of the ignition delay time when the ignition is abrupt, as herein [13,15]. Although the endwall pressure measurement can also be used to monitor ignition (since the mixtures employed herein are exothermic enough to see a significant pressure increase at the time of ignition) all but two of the ignition times were obtained from the $CH^\star$ traces. The onset of rapid $CH^\star$ formation, delineated by the intersection of the steepest slope of the $CH^\star$ increase with the initial (i.e., zero) value of $CH^\star$, defined the ignition delay time, as in Petersen et al. [13].

2.2. Results

A listing of all the ignition delay time results is given in Table 1. The temperatures ranged from 1042 to 1585 K, and the pressures ranged from 5.3 to 31.4 atm. Figures 2–7 present the results of the experiments in comparison to the predictions of the detailed mechanism, described at length in Section 3. For all mixtures and conditions, the effect of propane addition was to speed up the ignition process, thus producing shorter

Table 1
Data table; τ_{ign} in μs

Mixture	T, P (K, atm)	τ_{ign}	T, P (K, atm)	τ_{ign}
90/10%	1476, 10.0	65	1536, 8.5	35
$\phi = 0.5$	1302, 9.7	582	1428, 7.8	129
	1369, 9.8	250	1252, 30.6	462
	1202, 8.9	1678	1369, 29.4	157
	1281, 7.9	818	1294, 30.9	342
90/10%	1281, 8.9	760	1272, 8.0	972
$\phi = 1.0$	1318, 6.8	627	1201, 8.8	1918
	1465, 8.5	96	1415, 7.4	205
	1142, 16.0	2059	1117, 24.3	1561
	1253, 17.5	665	1170, 23.3	1042
	1234, 15.1	881	1193, 22.8	886
	1271, 18.0	520		
90/10%	1337, 8.4	546	1150, 31.7	907
$\phi = 2.0$	1242, 5.3	293	1190, 28.0	685
	1255, 8.2	1346	1232, 26.4	560
	1222, 8.6	1998	1285, 24.9	358
	1535, 5.5	111	1426, 22.3	110
90/10%	1209, 6.9	3246	1512, 5.8	154
$\phi = 3.0$	1282, 6.7	1162	1276, 18.7	531
	1297, 7.0	1016	1305, 17.6	458
	1359, 6.4	570	1072, 30.1	1725
	1407, 6.4	375	1138, 28.3	1095
80/20%	1051, 27.8	2253	1159, 24.6	894
$\phi = 0.5$	1092, 27.3	1465	1210, 23.5	500
	1123, 26.1	1261	1295, 23.9	201
70/30%	1128, 8.4	2070	1375, 7.7	145
$\phi = 1.0$	1133, 7.5	2611	1280, 29.1	168
	1244, 7.9	697	1503, 29.2	7
	1244, 8.7	634	1190, 31.4	382
	1295, 8.1	380	1241, 29.8	235
	1322, 10.7	234		
70/30%	1355, 7.3	297	1159, 8.1	1971
$\phi = 2.0$	1411, 6.2	182	1218, 27.2	277
	1585, 6.2	42	1142, 31.1	427
	1234, 8.4	938	1298, 26.1	145
	1269, 7.1	745	1298, 23.4	160
	1217, 9.0	1042	1284, 27.7	167
	1282, 8.1	524		
70/30%	1246, 7.8	494	1144, 27.1	497
$\phi = 3.0$	1167, 7.8	988	1112, 29.5	518
	1291, 7.6	350	1352, 20.3	131
	1276, 6.2	476	1028, 32.2	1131
	1353, 7.0	203	1122, 28.5	513
	1425, 6.5	114		
60/40%	1401, 9.1	80	1218, 15.5	397
$\phi = 0.5$	1237, 8.8	655	1042, 27.5	1811
	1256, 9.0	519	1085, 27.1	1253
	1202, 9.5	907	1125, 26.5	825
	1125, 9.5	1972	1164, 25.2	504
	1094, 16.6	1530	1211, 24.7	354
	1184, 16.3	651	1269, 23.8	201

The 12-atm, 80/20% data at $\phi = 0.5$ were originally presented in [13] and are not included in this table.

ignition delay times. As anticipated, increasing pressures also led to decreasing ignition times (Figs. 2–4).

3. Computational modeling

3.1. Background

As methane is the main component of natural gas and, being the simplest stable C_1 species, its oxidation mechanism forms the foundation for all other hydrocarbon mechanisms. There have been many detailed chemical modeling studies carried out on methane oxidation [16] culminating in the Gas Research Institute study [17]. The most recent mechanism (GRI-MECH 3.0), comprising 53 species and 322 reactions, was developed and published in a number of electronic versions [18] and was primarily constructed to describe the ignition of methane and natural gas.

In addition to the GRI study, there have been many other mechanisms developed to describe methane oxidation, but two in particular should be highlighted. Konnov [19] has published a purely electronic detailed reaction mechanism for methane and natural gas combustion which also deals with C_2 and C_3 hydrocarbons and their derivatives, N–H–O chemistry and NO_x formation in flames. More recently, Hughes et al. [20] have published a mechanism which describes the oxidation kinetics of hydrogen, carbon monoxide, methane, ethane and ethene in flames and homogeneous ignition systems. This Leeds mechanism (version 1.4) consists of 351 irreversible reactions of 37 species, built with an overall philosophy consistent with that of GRI-Mech. All three of the aforementioned mechanisms employ a large dataset of experiments including species profiles and ignition delay times in shock waves, laminar-flame species profiles, laminar flame speeds, and, temperature and stable species concentration profiles in flow reactors to validate their mechanisms, although, in the case of the Konnov mechanism, the bulk of the validating experiments are focussed on H_2, CO, N_2O, NO_2 and NH_3 kinetics and not on the hydrocarbons CH_4, C_2H_6, and C_3H_8. Included in these validations are studies of experiments on laminar flame speeds [21–28], ignition delay measurements [29–32] and species profiles in laminar flames [33].

Recently, Petersen et al. [34] conducted an analytical study to supplement extreme shock-tube measurements of CH_4/O_2 ignition at elevated pressures (4–26 MPa), high dilution (fuel plus oxidizer $\leqslant$30%), intermediate temperatures (1040–1500 K), and equivalence ratios as high as 6. A 38-species, 190-reaction model (RAMEC), based on GRI-Mech 1.2 [35], was developed using additional reactions that are important in methane oxidation at lower temperatures. The detailed-model calculations agree well with the measured ignition delay times and reproduce the accelerated ignition trends seen in the data at higher pressures and lower temperatures. Sensitivity and species flux analyses were

used to identify the primary reactions and kinetic pathways for the conditions studied. In general, reactions involving $H\dot{O}_2$, $CH_3\dot{O}_2$, and $H_2\dot{O}_2$ have increased importance at the conditions of this work relative to previous studies at lower pressures and higher temperatures. At a temperature of 1400 K and pressure of 10 MPa, the primary ignition promoters are:

$$\dot{C}H_3 + O_2 = O + CH_3\dot{O} \rightsquigarrow CH_2O + \dot{H}$$

$$\dot{C}H_3 + H\dot{O}_2 = CH_3\dot{O} + \dot{O}H$$

Methyl recombination to ethane is a primary termination reaction and is the major sink for $\dot{C}H_3$ radicals. At 1100 K, 10 MPa, the dominant chain-branching reactions become:

$$\dot{C}H_3 + CH_3\dot{O}_2 = CH_3\dot{O} + CH_3\dot{O}$$

$$H_2O_2 + M = \dot{O}H + \dot{O}H + M$$

These two reactions enhance the formation of $\dot{H}$ and $\dot{O}H$ radicals, explaining the accelerated ignition delay time characteristics at lower temperatures.

The Petersen et al. study highlights the need to include the $CH_3\dot{O}_2$ radical species and reactions in a reaction mechanism to correctly simulate methane oxidation chemistry under high-pressure, intermediate-temperature conditions. These conditions are important to natural gas oxidation in high-pressure combustors. The $CH_3\dot{O}_2$ radical species and reactions are not included in either GRI-MECH 3.0 or the Leeds mechanism. In addition, Petersen et al. did not extend their kinetic modelling study to include experimental results recorded in other physical systems (jet-stirred reactors, flow reactors, etc.) nor in other shock tubes. To this end, we have decided to generate a detailed chemical kinetic mechanism to describe methane oxidation over a wide range of conditions but which includes also the $CH_3\dot{O}_2$ radical species and its reactions.

3.2. Mechanism formulation

Modeling computations were carried out using the HCT modeling code [36]. In simulating shock-tube conditions, the thermal environment in the post-shock region can be safely assumed to be adiabatic. In addition, the short reaction time scales relative to diffusive times permits the zero-dimensional approximation. The treatment of the free boundary of the reaction zone is open to some debate as to whether a constant volume or constant pressure assumption better describes the region behind the reflected shock wave. The limiting case used in this study assumes a constant-volume (density) boundary, which implies that the bulk expansion of the fluid due to temperature rise and average molecular weight change overwhelms the inertial effects of the surrounding fluid.

The detailed chemical kinetic reaction mechanism used in these calculations was based on the hierarchical nature [37] of reacting systems. The hydrogen submechanism is based on that which has recently been validated by Ó Conaire et al. [38] in the temperature range 298–2700 K, at pressures from 0.05 to 87 atm, and equivalence ratios from 0.2 to 6.0. The kinetic mechanism employed for the methane/ethane system is based on that published by Fischer et al. [39] in their dimethyl ether study.

The C_3 submechanism is based on the modeling work of Curran et al. [40,41] using the thermochemical parameters and rate constant rules described in their work on *iso*-octane oxidation. The complete kinetic mechanism consists of 118 different chemical species and 663 elementary reactions and is available by writing to the authors (henry.curran@nuigalway.ie).

Modifications have been made to some of the methane chemistry with some of the more significant changes discussed here. For the reactions:

$$\dot{C}H_3 + O_2 \rightarrow CH_3\,\dot{O}_2$$

$$\dot{C}H_3 + O_2 \rightarrow CH_3\dot{O} + \dot{O}$$

$$\dot{C}H_3 + O_2 \rightarrow CH_2O + \dot{O}H$$

the recommendations from the *ab initio* study of Zhu et al. [42] have been employed for the association reaction generating the $CH_3\dot{O}_2$ radical. We have also included an analysis to account for pressure dependence using quantum Rice–Ramsperger–Kassel theory with a master equation analysis [43]. The output from this code was used to generate a Troe fit (A. Kazakov, Private Communication, 2000) of the data. Rate constants for the reactions producing $CH_3\dot{O} + \dot{O}$ and

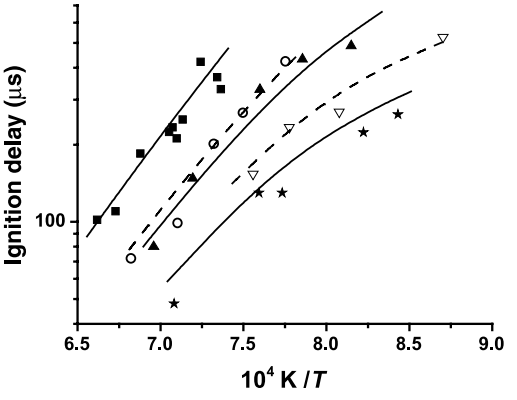

Fig. 1. Experimental results [34] (symbols) versus model predictions (lines) at 20% CH_4, 13.3% O_2, 66.7% N_2, $\phi = 3.0$, ■ $P_5 \approx 40$ atm, ○ $P_5 \approx 75$ atm, ▲ $P_5 \approx 85$ atm, ▽ $P_5 \approx 115$ atm, ★ $P_5 \approx 140$ atm. Dashed line corresponds with open symbols.

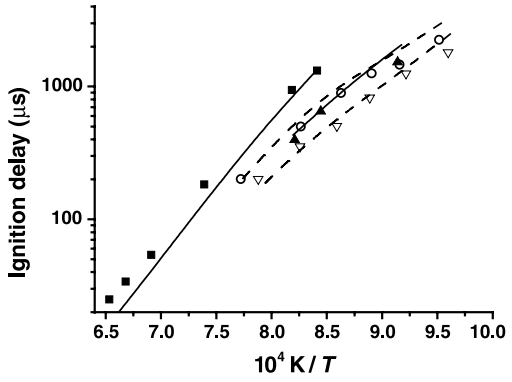

Fig. 2. Experimental results (this study and [13]; symbols) versus model predictions (lines) at $\phi = 0.5$, (80% CH_4/20% C_3H_8), ■ $P_5 \approx 12$ atm, ○ $P_5 \approx 26$ atm, (60% CH_4/40% C_3H_8), ▲ $P_5 \approx 16$ atm, ▽ $P_5 \approx 26$ atm. Dashed lines correspond with open symbols.

$CH_2O + \dot{O}H$ are based on the analysis of Zhu et al. [42] together with the more recent work of Herbon et al. [44] and Srinivasan et al. [45]. The greatest difference in rate constant lies in the channel producing $CH_2O + \dot{O}H$. The most recent recommendation of Srinivasan et al. is seven times faster than that recommended by Herbon et al. at 1000 K. We have taken an "average" of these two recommendations using a rate constant of 5.87×10^{11} exp($-13{,}840$ cal mol^{-1}/RT) cm^3 mol^{-1} s^{-1}.

The rate constant for the reaction:

$$\dot{C}H_3\dot{O}_2 + \dot{C}H_3 \rightarrow CH_3\dot{O} + CH_3\dot{O}$$

has been estimated to be 1.0×10^{13} exp(-1000 cal mol^{-1}/RT) cm^3 mol^{-1} s^{-1} to simulate correctly experimental ignition delay times under high-pressure and low- to intermediate-temperature conditions.

In addition, the rate constants for the reactions

$$\dot{C}H_3 + H\dot{O}_2 \rightarrow CH_3\dot{O} + OH$$

$$\dot{C}H_3 + H\dot{O}_2 \rightarrow CH_4 + O_2$$

have been altered such that the chain branching reaction is 2.8 times faster than the chain termination pathway. In the study by Fischer et al. [39], this branching ratio was 3.67.

3.3. Simulations

The detailed chemical kinetic mechanism has been validated against a wide range of available data in the literature. Recently Dagaut and Dayma [46] studied the oxidation of hydrogen/natural gas mixtures in a fused silica jet-stirred reactor operating at 10 atm, over the temperature range 900–1200 K for equivalence ratios of 0.3, 0.6, and 1. The concentration profiles of the reactants, stable intermediates and the final products were measured by probe sampling followed by on-line FTIR analyses and off-line GC-TCD/FID analyses. These data have been successfully simulated using the detailed mechanism, but due to space limitations the comparisons are available as Supplementary material.

Petersen et al. [34] conducted an analytical study to supplement extreme shock-tube measurements of CH_4/O_2 ignition at elevated pressures (40–260 bar), high dilution (fuel plus oxidizer $\leqslant$30%), intermediate temperatures (1040–1500 K), and equivalence ratios as high as 6. Figure 1 shows a comparison of model-predicted versus experimentally measured ignition delay

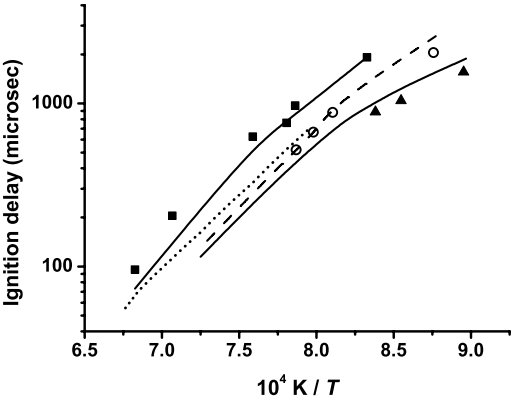

Fig. 3. Experimental results (this study; symbols) versus model predictions (lines) at $\phi = 1.0$ (90% CH_4/10% C_3H_8), ■ $P_5 \approx 8.1$ atm, ○ $P_5 \approx 16.6$ atm, ▲ $P_5 \approx 23.5$ atm. Dashed line corresponds with open symbols. Dotted line: fit to 8 atm data using correlation of Spadaccini and Colket [2].

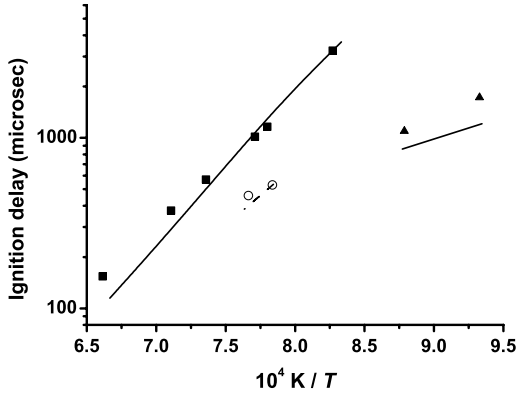

Fig. 4. Experimental results (this study; symbols) versus model predictions (lines) at $\phi = 3.0$ (90% CH_4/10% C_3H_8), ■ $P_5 \approx 6.0$ atm, ○ $P_5 \approx 18.0$ atm, ▲ $P_5 \approx 29.0$ atm. Dashed line corresponds with open symbols.

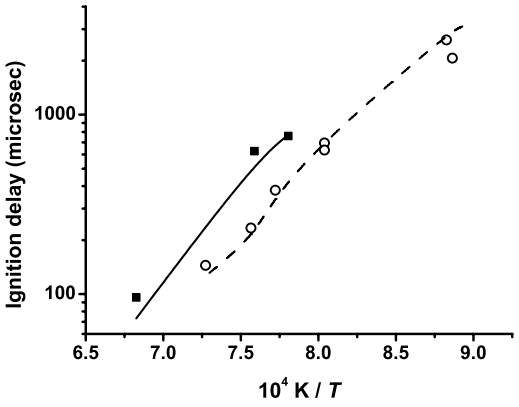

Fig. 5. Experimental results (this study; symbols) versus model predictions (lines) at $\phi = 1.0$, $P_5 \approx 8.0$ atm, ■ 90% CH_4/10% C_3H_8, ○ 70% CH_4/30% C_3H_8. Dashed line corresponds with open symbols.

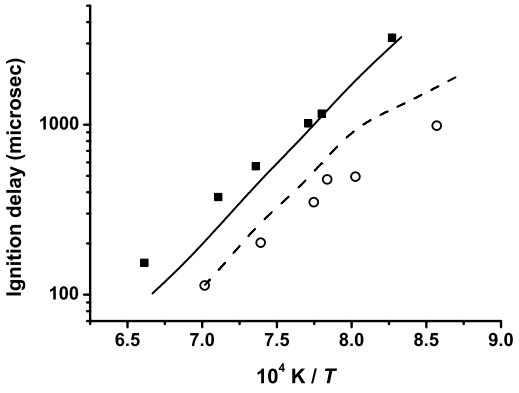

Fig. 6. Experimental results (this study; symbols) versus model predictions (lines) at $\phi = 3.0$, $P_5 \approx 7.0$ atm, ■ 90% CH_4/10% C_3H_8, ○ 70% CH_4/30% C_3H_8. Dashed line corresponds with open symbols.

times for a 20% CH_4, 13.3% O_2 ($\phi = 3.0$) mixture at reflected-shock pressures of 40, 75, 85, 115, and 140 atm. Good agreement is observed between model and experiment, although the model is slower than experiment for the highest-pressure (140 atm) measurements.

Figure 2 shows a comparison of experimental results versus model predictions for two fuel–lean mixtures ($\phi = 0.5$); one with 80% CH_4/20% C_3H_8 and the second with 60% CH_4/40% C_3H_8 in air at reflected-shock pressures of 12 and 26 atm for the 80/20% mixture and 16 and 26 atm for the 60/40% mixture. The data at 12 atm and 16 atm cannot be compared directly, but at 26 atm a direct comparison can be made. The 60% CH_4/40% C_3H_8 mixture is clearly faster to ignite than the 80% CH_4/20% C_3H_8 mixture, and this behavior is also accurately captured by the kinetic mechanism.

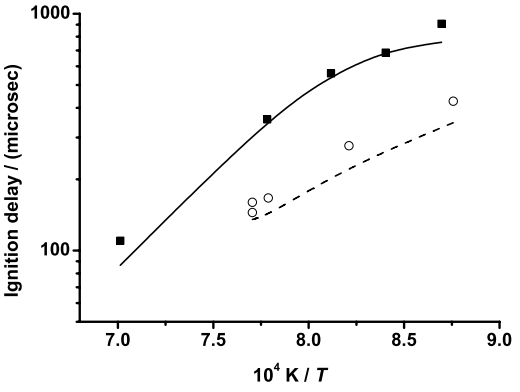

Fig. 7. Experimental results (this study; symbols) versus model predictions (lines) at $\phi = 2.0$, $P_5 \approx 27.0$ atm, ■ 90% CH_4/10% C_3H_8, ○ 70% CH_4/30% C_3H_8. Dashed line corresponds with open symbols.

Figure 3 shows a comparison of experimental results versus model predictions for a 90% CH_4/10% C_3H_8 mixture at $\phi = 1.0$ in air at reflected-shock pressures of approximately 8.0, 16.5, and 23.5 atm. The mechanism is in good agreement with experiment at 8 and 16.5 atm but is consistently 20% slower at the highest shock pressure of 23.5 atm, which also corresponds to the lowest-temperature measurements. However, the measured lower activation energy for oxidation at temperatures below 1200 K, which is particularly obvious for the 23.5 atm data, is well reproduced by the model. Also shown in Fig. 3 is a comparison between the present data and the data of Spadaccini and Colket [2]. Their data at $\phi = 1.0$ with propane addition are represented by their correlation, plotted for the 90/10% mixture at a pressure of 8.1 atm. This is a fair comparison since their data cover a range of pressures around 6–8 atm for a slightly lower level of propane addition (6%) and for temperatures above 1300 K. The Spadaccini and Colket correlation tends to overestimate the reduction in ignition time for the 10% addition of the new data although there is good agreement in the activation energies.

A similar comparison is shown in Fig. 4 for a fuel-rich equivalence ratio of three for a 90% CH_4/10% C_3H_8 mixture at three different average pressures: 6, 18, and 29 atm. There is excellent agreement between model and experiment for this mixture at 6 and 18 atm, with the model underpredicting slightly the ignition time at the highest temperature near 1500 K. At 29 atm, the model begins to underpredict ignition delay time slightly.

Figures 5 and 6 show the effect of increasing propane addition for fixed equivalence ratios of 1.0 and 3.0, respectively. In Fig. 5, the effect of increasing the propane from 10% to 30% of the fuel blend at 8 atm and $\phi = 1.0$ is to decrease

the ignition delay time, as expected. There is very good agreement between the mechanism and the data for these mixtures. For the $\phi = 3.0$ mixtures in Fig. 6, the model tends to overpredict the ignition time slightly for the 30% propane case and underpredict it slightly for the 10% case. Nonetheless, the relative effect of propane addition is still captured very well. Similar results are seen for the $\phi = 2.0$ mixtures in Fig. 7.

Output reaction edits from HCT were analyzed for an 80% CH_4/20% C_3H_8 mixture at $\phi = 0.5$ in air at reflected-shock pressures of approximately 26 atm at a time at which 11% CH_4 had been consumed, corresponding to approximately 62% C_3H_8 consumption. It was found that methane and propane undergo abstraction mainly by hydroxyl radicals (≈70%) with the remainder by H· and Ȯ atoms and $H\dot{O}_2$ radicals. Hydroxyl radicals are formed via:

$$H_2O_2(+M) \xrightarrow{53} \dot{O}H + \dot{O}H(+M)$$

$$\dot{C}H_3 + H\dot{O}_2 \xrightarrow{12} CH_3\dot{O} + \dot{O}H$$

$$\dot{C}_3H_5 - a + H\dot{O}_2 \xrightarrow{7} C_3H_5\dot{O} + \dot{O}H$$

$$\dot{C}H_3 + O_2 \xrightarrow{6} CH_2O + \dot{O}H$$

where the number over the arrow indicates the percentage ȮH being formed via that channel.

Methyl radicals react with hydroperoxyl radicals to produce a methoxy and an hydroxyl radical (44%) as indicated above or can also react via the termination reaction producing methane and molecular oxygen (20%). Methyl radicals also combine with molecular oxygen producing stabilized methyl peroxyl radicals (23%) which react with methyl radicals to produce two methoxy radicals. These then either undergo β-scission to formaldehyde and a H· atom (60%) or react with molecular oxygen to produce formaldehyde and a hydroperoxyl radical (40%).

$$\dot{C}H_3 + H\dot{O}_2 \xrightarrow{44} CH_3\dot{O} + \dot{O}H$$

$$\dot{C}H_3 + O_2(+M) \xrightarrow{23} CH_3\dot{O}_2(+M)$$

$$\dot{C}H_3 + H\dot{O}_2 \xrightarrow{20} CH_4 + O_2$$

$$\dot{C}H_3 + CH_2O \xrightarrow{14} CH_4 + H\dot{C}O$$

$$CH_3\dot{O}_2 + \dot{C}H_3 \rightarrow CH_3\dot{O} + CH_3\dot{O}$$

$$CH_3\dot{O}(+M) \xrightarrow{60} CH_2O + \dot{H}(+M)$$

$$CH_3\dot{O} + O_2 \xrightarrow{40} CH_2O + H\dot{O}_2$$

Acknowledgments

This work was supported primarily by Rolls-Royce Canada Ltd. Partial support for the experiments came from The Aerospace Corporation. The authors gratefully acknowledge the assistance of Carrol Gardner in the laboratory.

Appendix A. Supplementary data

Supplementary data associated with this article can be found in the online version at doi:10. 1016/j.proci.2006.08.034.

References

[1] A.H. Lefebvre, *Gas Turbine Combustion*, second ed., Taylor & Francis, Philadelphia PA, 1999.
[2] L.J. Spadaccini, M.B. Colket III, *Prog. Energy Combust. Sci.* 20 (5) (1984) 431–460.
[3] J.D. Naber, D.L. Siebers, S.S. Di Julio, C.K. Westbrook, *Combust. Flame* 99 (1994) 192–200.
[4] R.M. Flores, M.M. Miyasato, V.G. McDonell, G.S. Samuelsen, *J. Eng. Gas Turb. Power* 123 (2001) 824–831.
[5] R.M. Flores, V.G. McDonell, G.S. Samuelsen, *J. Eng. Gas Turb. Power* 125 (2003) 701–708.
[6] A. Lifshitz, K. Scheller, A. Burcat, G.B. Skinner, *Combust. Flame* 16 (1971) 311–321.
[7] R.W. Crossley, E.A. Dorko, K. Scheller, A. Burcat, *Combust. Flame* 19 (1972) 373–378.
[8] C.S. Eubank, M.J. Rabinowitz, W.C. Gardiner Jr., R.E. Zellner, *Proc. Combust. Inst.* 18 (1981) 1767–1774.
[9] R. Zellner, K.J. Niemitz, J. Warnatz, W.C. Gardiner Jr., C.S. Eubank, J.M. Simmie, *Prog. Aeronaut. Astronaut.* 80 (1983) 252–272.
[10] M. Frenklach, D.E. Bornside, *Combust. Flame* 56 (1984) 1–27.
[11] N. Lamoureux, C.-E. Paillard, *Shock Waves* 13 (2003) 57–68.
[12] J. Huang, W.K. Bushe, *Combust. Flame* 144 (2006) 74–88.
[13] E.L. Petersen, J.M. Hall, S.D. Smith, J. de Vries, A. Amadio, M.W. Crofton, *ASME Paper* GT2005-68517, 2005.
[14] E.L. Petersen, M.J.A. Rickard, M.W. Crofton, E.D. Abbey, M.J. Traum, D.M. Kalitan, *Meas. Sci. Technol.* 16 (2005) 1716–1729.
[15] M.J.A. Rickard, J.M. Hall, E.L. Petersen, *Proc. Combust. Inst.* 30 (2005) 1915–1923.
[16] J.M. Simmie, *Prog. Energy Comb. Sci.* 29 (2003) 599–634.
[17] G.P. Smith, D.M. Golden, M. Frenklach, et al., GRI-Mech 3.0. Available at <http://www.me.berkeley.edu/gri_mech>.
[18] Versions 1.2 and 2.11 available at <http://web.galcit.caltech.edu/EDL/mechanisms>.
[19] A. Konnov, 2000, Version 0.5. Available at <http://homepages.vub.ac.be/~akonnov>.
[20] K.J. Hughes, T. Turányi, A.R. Clague, M.J. Pilling, *Int. J. Chem. Kinet.* 33 (2001) 513–538.
[21] F.N. Egolfopoulos, C.K. Law, *Proc. Combust. Inst.* 23 (1990) 333–340.
[22] D.R. Dowdy, D.B. Smith, S.C. Taylor, A. Williams, *Proc. Combust. Inst.* 23 (1990) 325–332.
[23] F.N. Egolfopoulos, D.L. Zhu, C.K. Law, *Proc. Combust. Inst.* 23 (1990) 471–478.

[24] S.C. Taylor, Ph.D. thesis, University of Leeds, 1991.
[25] C.M. Vagelopoulos, F.N. Egolfopoulos, C.K. Law, *Proc. Combust. Inst.* 25 (1994) 1341–1347.
[26] A. Van Maaren, D.S. Thung, L.P.H. De Goey, *Combust. Sci. Tech.* 96 (1994) 327–344.
[27] I.C. Mclean, D.B. Smith, S.C. Taylor, *Proc. Combust. Inst.* 25 (1994) 749–757.
[28] K.T. Aung, M.I. Hassan, G.M. Faeth, *Combust. Flame* 109 (1997) 1–24.
[29] T. Asaba, W.C. Gardiner Jr., R.F. Stubbeman, *Proc. Combust. Inst.* 10 (1965) 295–302.
[30] T. Tsuboi, H.Gg. Wagner, *Proc. Combust. Inst.* 15 (1974) 883–890.
[31] D.J. Seery, C.T. Bowman, *Combust. Flame* 14 (1970) 37–47.
[32] K. Takahashi, T. Inomata, T. Moriwaki, S. Okazaki, *Bull. Chem. Soc. Japan* 62 (1989) 2138–2145.
[33] J.S. Bernstein, A. Fein, J.B. Choi, et al., *Combust. Flame* 92 (1993) 85–105.
[34] E.L. Petersen, D.F. Davidson, R.K. Hanson, *J. Propul. Power* 15 (1999) 82–91.
[35] M. Frenklach, H. Wang, C.L. Yu, et al., GRI-Mech version 1.2, 1995.
[36] C.M. Lund, L. Chase, Lawrence Livermore National Laboratory report UCRL-52504, revised, 1995.
[37] C.K. Westbrook, F.L. Dryer, *Prog. Energy Combust. Sci.* 10 (1) (1984) 1–57.
[38] M. O'Conaire, H.J. Curran, J.M. Simmie, W.J. Pitz, C.K. Westbrook, *Int. J. Chem. Kinet.* 36 (2004) 603–622.
[39] S.L. Fischer, F.L. Dryer, H. J Curran, *Int. J. Chem. Kinet.* 32 (2000) 713–740.
[40] H.J. Curran, P. Gaffuri, W.J. Pitz, C.K. Westbrook, *Combust. Flame* 114 (1998) 149–177.
[41] H.J. Curran, P. Gaffuri, W.J. Pitz, C.K. Westbrook, *Combust. Flame* 129 (2002) 253–280.
[42] R. Zhu, C.-C. Hsu, M.C. Lin, *J. Chem. Phys.* 115 (2001) 195–203.
[43] C. Sheng, J.W. Bozzelli, A.M. Dean, A.Y. Chang, *J. Phys. Chem. A* 106 (31) (2002) 7276–7293.
[44] J.T. Herbon, R.K. Hanson, C.T. Bowman, D.M. Golden, *Proc. Combust. Inst.* 30 (2005) 955–963.
[45] N.K. Srinivasan, M.C. Su, J.W. Sutherland, J.V. Michael, *J. Phys. Chem. A* 109 (35) (2005) 7902–7914.
[46] P. Dagaut, G. Dayma, *Int. J. Hydrogen Energy* 31 (4) (2006) 505–515.

Comments

Ken Brezinsky, University of Illinois at Chicago, USA. From my perspective 30 atm is not high pressure but "low" pressure. I say that because our work on CO oxidation at pressures above 200 atm revealed, because of the high pressure, that the Davis et al. model of 2005 needed some adjustment. Do you expect to do higher pressure experiments to probe this model more?

Reply. Higher-pressure experiments would certainly produce data that will likely challenge the current model, eventually leading to further improvement and additional insight. The range of pressures in the present study is in the range of most power generation gas turbine applications, and we bracketed the test pressures with this range in mind. Since our present facility is rated for reflected-shock pressures as high as 100 atm, we could certainly, in the future, probe to higher pressures, although there are no immediate plans to do so for these mixtures. One thing we need to be careful about is the fact that the undiluted fuel–air mixtures utilized herein are quite exothermic, leading to significant overpressures when strong ignition occurs, making the peak pressure in the experiment several times higher than the original pre-ignition pressure. Facility limitations and the strong ignition overpressure tend to set the limits on the pre-ignition (i.e., post-shock) pressure.

•

Anthony Dean, Colorado School of Mines, USA. Did you account for the pressure dependence of:

$$CH_3 + O_2 \rightarrow CH_3O + O$$
$$CH_3 + O_2 \rightarrow CH_2O + OH$$

Reply. We have included pressure effects in considering the reaction $CH_3O_2 + M = CH_3 + O_2$ (+M). However, in order to include pressure effects in the pathways leading to the formation of both $CH_2O + OH$ and $CH_3O + O$ we would have to include the isomerization reaction $CH_3O_2 \rightleftharpoons CH_2OOH$, with the adduct CH_2OOH leading to the formation of $CH_2O + OH$. This reaction would also have to be pressure dependant, and we have not included this analysis as yet. Our current rate expressions are based on measurements taken at approximately 1 atm.